This is the accepted version of the article: Garzón Tovar, Luis, et al. *Spray drying for making covalent chemistry II: synthesis of covalent-organic framework superstructures and related composites* in Chemical communications, vol. 53, issue 82 (Oct. 2017), p. 11372-11375.

Available at: https://dx.doi.org/10.139/c7cc07052g

This version is published under a “All rights reserved” license.

Journal Name

COMMUNICATION

# Spray Drying for Making Covalent Chemistry II: Synthesis of Covalent–Organic Framework Superstructures and related Composites †

Received 00th January 20xx,
Accepted 00th January 20xx

DOI: 10.1039/x0xx00000x

www.rsc.org/

Luis Garzón-Tovar,[a] Ceren Avci-Camur,[a] David Rodríguez-San-Miguel,[b] Inhar Imaz,[a] Félix Zamora*[b,c] and Daniel Maspoch*[a,d]

**Here we report a method that combines the spray-drying technique with a dynamic covalent chemistry process to synthesize zero-dimensional, spherical and microscale superstructures made from the assembly of imine-based COF nanocrystals. This methodology also enables the integration of other functional materials into these superstructures forming COF-based composites.**

Covalent Organic Frameworks (COFs) are an emerging class of crystalline porous materials, where two-dimensional (2D) or three-dimensional (3D) architectures are formed from organic building blocks linked by dynamic covalent bonds (*e.g.* imine, boroxine, β-keto-enamine and azine).[1-3] These materials are characterized by their high porosity, high thermal stability and low mass density, which confer them potential for myriad applications, such as gas sorption and storage,[4-7] catalysis,[8-10] sensors[11-13] and optoelectronics.[14, 15] Seeking to exploit these possibilities, researchers have developed several fabrication methods for COFs, including not only the traditional solvothermal synthesis but also microwave,[16] microfluidic,[17] mechanochemical,[18] ionothermal,[19] and continuous-flow synthesis.[20, 21]

While many efforts have been devoted to the synthesis of new COFs and to their production methods, there is a growing interest in structuring these COFs at the micro/macroscopic scale forming more complex, high-order super- or mesostructures from the assembly of COF nanoparticles. As their Metal-Organic Framework (MOF) counterparts,[22, 23] these type of structures made from COF nanocrystals are especially attractive due to the possibility of (i) controlling the shaping and sizing of COFs at the micro/macroscale, two parameters that are very important to control for many applications; (ii) enhancing the initial performance *via* design of their morphology; and (iii) combining COFs with other materials to create functional composites, which can further expand the scope for applications.[24-27]

To date, there are a few studies based on the creation of COF superstructures. For example, Banerjee *et al*. synthesized a highly crystalline and porous COF in the form of hollow spheres that were used for immobilizing the enzyme trypsin.[28] In a more recent study, core-shell microspheres containing $Fe_3O_4$ nanoclusters were synthesized using a template assisted route. The resulting hybrid microspheres showed photothermal conversion ability after exposing them to near infrared light.[25]

Despite these advances, synthesis of higher-order COF superstructures is still challenging mainly due to the harsh conditions usually needed to synthesize highly crystalline COF nanoparticles. In these sense, we have recently reported that the spray drying method can be used to synthesize MOFs in the form of spherical hollow or compact superstructures made from the assembly of MOF nanoparticles.[29-32] Additionally, we have recently reported that spray drying is also an effective methodology to perform Schiff-base condensation reactions, either between discrete organic molecules or on the pore surfaces of MOFs.[33] Herein, we combine both achievements and extend the applicability of spray drying to synthesize imine-based COF nanocrystals while structuring them into spherical hollow superstructures. This strategy consists in a two-step process. In a first step, the spray drying allows the formation and shaping of amorphous imine-based polymer spheres. Then, in a second step, these spheres are subjected to a dynamic covalent chemistry to crystallize them under similar conditions to those reported by Dichtel *et al*.[34] Remarkably, after the crystallization step, the resulting superstructures preserve the initial size and morphology of the amorphous spheres. Further,

[a] Catalan Institute of Nanoscience and Nanotechnology (ICN2), CSIC and The Barcelona Institute of Science and Technology, Campus UAB, Bellaterra, 08193 Barcelona, Spain
Email: daniel.maspoch@icn2.cat
[b] Departamento de Química Inorgánica and Institute for Advanced Research in Chemical Sciences (IAdChem), Universidad Autónoma de Madrid, Madrid, 28049, Spain
Email: felix.zamora@uam.es
[c] Instituto Madrileño de Estudios Avanzados en Nanociencia (IMDEA Nanociencia), Cantoblanco, 28049, Madrid, Spain
[d] ICREA, Pg. Lluís Companys 23, 08010 Barcelona, Spain

† Electronic Supplementary Information (ESI) available: Experimental procedures and additional characterization of the synthesized COFs. See DOI: 10.1039/x0xx00000x

Please do not adjust margins



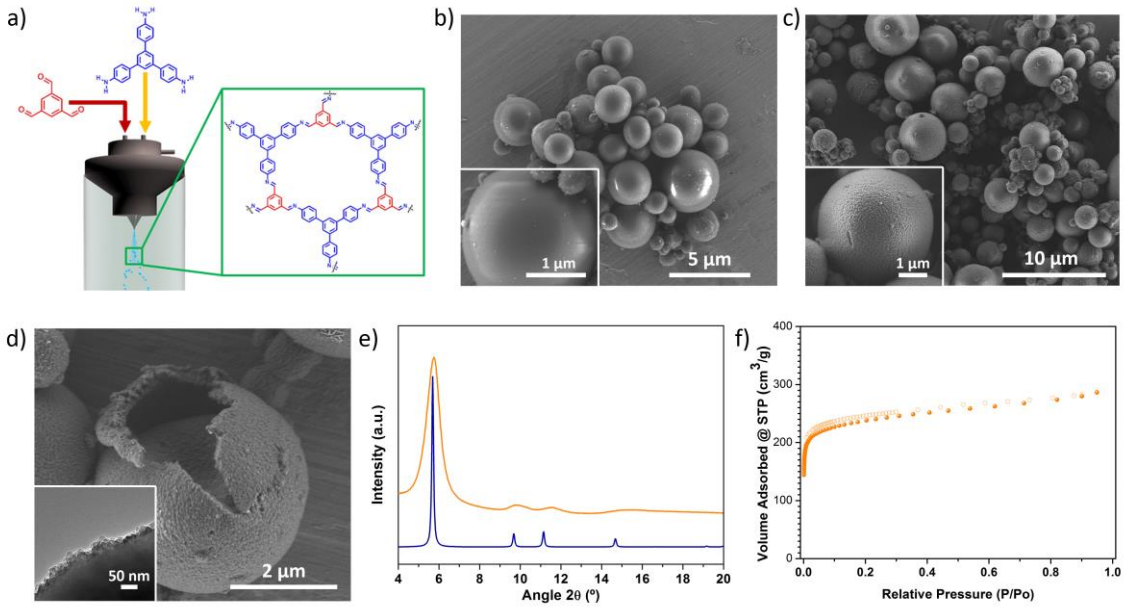


Figure 1. a) Schematic representation of the spray drying synthesis of **COF-TAPB-BTCA**. b) Representative FESEM images of amorphous **COF-TAPB-BTCA** spheres. c) Representative FESEM images of microspherical **COF-TAPB-BTCA** superstructures d) FESEM and HRTEM images of a mechanically broken superstructure, revealing the hollow cavity and that they are formed by COF nanocrystals. e) XRPD diffractogram of **COF-TAPB-BTCA** (orange), compared with the simulated powder pattern (blue). f) $N_2$ adsorption isotherm of **COF-TAPB-BTCA**.

we show that this strategy enables integrating guest functional materials, either molecules or other nanomaterials, in these COF superstructures.

Initially, we began with the synthesis of superstructures of **COF-TAPB-BTCA**, a two-dimensional COF assembled from two trigonal building blocks, 1,3,5-benzenetricalbaldehyde (BTCA) and 1,3,5-tris-(4-aminophenyl)benzene (TAPB).[35] In a typical first step, a 0.03 mol·L$^{-1}$ solution of BTCA in a mixture of DMSO and acetic acid (9:1 v/v) and a 0.03 mol·L$^{-1}$ solution of TAPB in DMSO were independently atomized using a three-fluid nozzle at a feed rate of 3.0 mL·min$^{-1}$, a flow rate of 336 mL·min$^{-1}$ and an inlet temperature of 200 °C, using a B-290 Mini Spray Dryer (BÜCHI Labortechnique). This atomization immediately afforded a yellow powder (Figure 1a). Note here that the use of three-fluid nozzle ensured that the two reactants only come in contact inside the drying chamber avoiding the clogging of the nozzle.

Field-emission scanning electron microscopy (FESEM) images and X-ray powder diffraction (XRPD) performed on the intermediate collected solid revealed the homogeneous formation of amorphous spheres with an average size of 2.2 ± 1.1 µm (Figure 1b and S1 ESI†). Since the spray-drying is based on the fast evaporation of the solvent, we reasoned that the kinetic product was obtained instead of thermodynamic one. The formation of the imine-based polymer was confirmed by FT-IR spectroscopy and solid-state $^{13}$C magic angle spinning nuclear magnetic resonance (MAS NMR). The FT-IR spectrum showed the presence of the typical imine (C=N) band at 1633 cm$^{-1}$ and the absence of the band corresponding to free -$NH_2$ between 3300-3500 cm$^{-1}$, indicating the absence of unreacted TAPB. The imine formation was further corroborated by the appearance of a signal at 158 ppm in the $^{13}$C MAS NMR spectrum, which was attributed to the carbon atom of the C=N imine group (Figure S2, ESI†). These results are in agreement

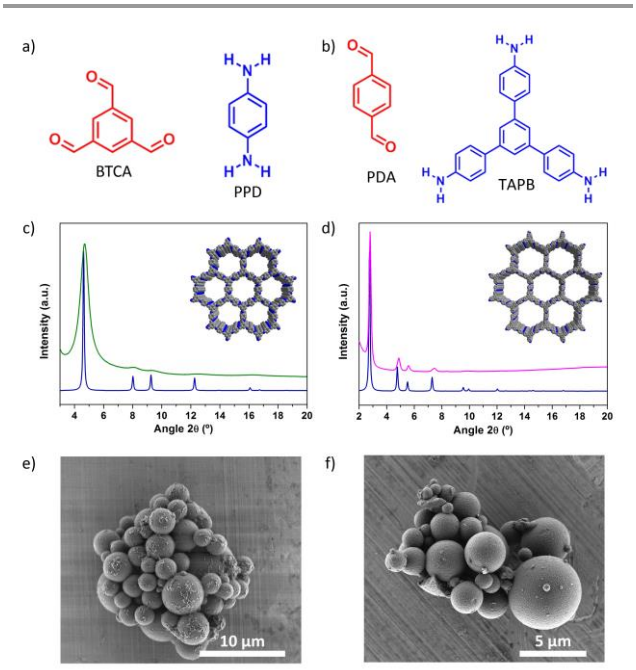


Figure 2. a,b) Representation of the building blocks used to synthesize (a) **COF-LZU1** and (b) **COF-TAPB-PDA**. c) XRPD diffractogram of the obtained **COF-LZU1** (green) compared with simulated powder pattern (blue). d) XRPD diffractogram of the obtained **COF-TAPB-PDA** (pink) compared with simulated powder pattern (blue). e,f) FESEM images showing the general view of the microspherical (e) **COF-LZU1** and (f) **COF-TAPB-PDA** superstructures.



This journal is © The Royal Society of Chemistry 20xx

Please do not adjust margins

Please do not adjust margins



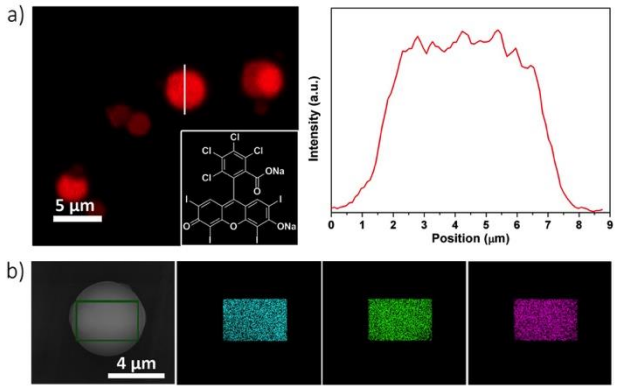


Figure 3. a) Confocal fluorescence image of **Rose-bengal@COF-TAPB-BTCA** superstructures and their fluorescence intensity profile. Inset: chemical structure of rose Bengal. b) Elemental mapping with EDX performed on a single spherical superstructure of **Rose-bengal@COF-TAPB-BTCA**, showing the homogeneous distribution Na (cyan), Cl (green) and I (pink).

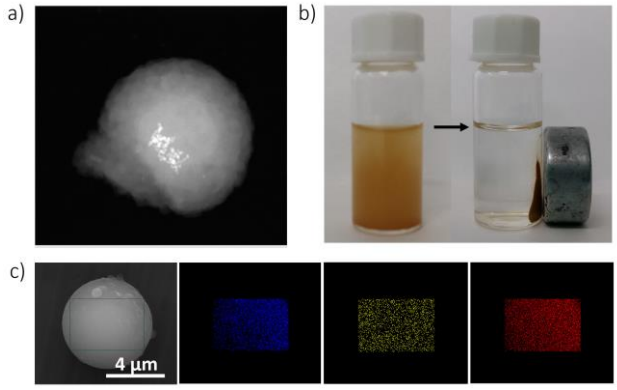


Figure 4. a) HAADF-STEM image of single **$Fe_3O_4$@COF-TAPB-BTCA** superstructure. b) Photographs of the dispersion of **$Fe_3O_4$@COF-TAPB-BTCA** superstructures before and after exposed to a magnet. c) Elemental mapping with EDX performed on a single spherical superstructure of **$Fe_3O_4$@COF-TAPB-BTCA**, showing the homogeneous distribution of N (blue), Fe (yellow) and O (red).

with those previously reported for **COF-TAPB-BTCA**.[35] In a second step, this imine-based polymer was subjected to a dynamic covalent chemistry process. Thus, the amorphous spheres were dispersed in a mixture of 1,4-dioxane/mesitylene/water/acetic acid and heated at 80 °C for 192 h. The isolated material did not show significant spectroscopic changes in both FT-IR and $^{13}C$ MAS NMR spectra (Figure S3, ESI†). However, FESEM and High-resolution transmission electron microscopy (HR-TEM) images displayed the formation of hollow superstructures in which their walls are created by the close packing of COF nanoparticles (Figure 1c-d and Figure S4, ESI†). Remarkably, these superstructures retained both shape and size of the amorphous spheres (Figure S5, ESI†). The XRPD pattern of these superstructures showed the most intense peak at 5.5°, which properly match with the simulated **COF-TAPB-BTCA** structure (Figure 1e and Figure S6, ESI†). The microporosity of the **COF-TAPB-BTCA** superstructures was confirmed by $N_2$ adsorption measurements, which gave a BET surface area of 911 $m^2 g^{-1}$. This value is consistent with that previously reported for **COF-TAPB-BTCA** (Figure 1f).[30] Finally, thermogravimetric analysis (TGA) revealed the high thermal stability of **COF-TAPB-BTCA** superstructures (up to 500 °C), following by a loss weight due to the decomposition of the framework (Figure S7, ESI†).

To demonstrate the generality of our approach, we used similar synthetic conditions to synthesize other imine-based COF superstructures. To this end, we selected the recently discovered **COF-LZU1**[8] and **COF-TAPB-PDA**.[34] **COF-LZU1** was synthesized by the condensation of BTCA and *p*-phenylenediamine (PPD), whereas **COF-TAPB-PDA** was synthesized from TAPB and terephthalaldehyde (PDA). In both cases, after the two-step process, FESEM and HR-TEM images and XRPD of the resulting solids revealed the formation of crystalline microspherical superstructures of the desired COFs (Figure 2 and Figure S8 and S9, ESI†). FT-IR spectra of **COF-LZU1** and **COF-TAPB-PDA** showed the presence of the characteristic C=N stretching band at 1618 and 1628 $cm^{-1}$, respectively. Moreover, the formation of imine was further corroborated by the peaks observed in the $^{13}C$ MAS NMR spectra at 157 ppm for **COF-LZU1** and 158 ppm for **COF-TAPB-PDA** (Figure S10 and S11, ESI†). Additionally, the microporosity of the COFs was confirmed by $N_2$ adsorption analysis, from which BET surface areas of 319 $m^2 g^{-1}$ for **COF-LZU1** and 1162 $m^2 g^{-1}$ for **COF-TAPB-PDA** were calculated (Figure S12, ESI†). These values are consistent with those previously reported.[8, 34]

Having demonstrated that our spray-drying methodology enables the formation of hollow COF superstructures, we envisioned to use it as a simple method for integrating other functional substances to these superstructures and thus, create COF-based composites.[36-38] To explore this possibility, we synthesized **Rose-bengal@COF-TAPB-BTCA** superstructures by reproducing the formation of **COF-TAPB-BTCA** superstructures but dissolving Rose bengal in the initial precursor solution. FESEM images and XRPD patterns revealed the formation of crystalline microspherical superstructures of **COF-TAPB-BTCA**, confirming that their synthesis was not affected by the presence of the dye (Figure S13, ESI†). The presence of Rose bengal was confirmed by elemental mapping with energy dispersive X-ray spectrometry (EDX) performed on a single superstructure, which revealed a highly uniform distribution of Cl, I, and Na atoms (Figure 3b). Additionally, the successful encapsulation of this dye was visualized by confocal images, where the intensity profile and the confocal image performed on a single sphere revealed the homogeneous distribution of Rose bengal (Figure 3a). Finally, to evaluate the possibility to release encapsulated molecules from these COF superstructures, Rose-bengal@COF-TAPB-BTCA composite was incubated in ethanol for different periods of time, and the dye released was quantified by Fluorescence spectroscopy (Figure S14, ESI†). Notably, a dye release of 32 % was observed for the first day, achieving a release of 56 % after 8 days. This slow release suggests that the dye is in fact located on the pores of the COF nanocrystals rather than on their crystal surface .

To further explore the formation of COF-based composites using this strategy, we incorporated magnetic $Fe_3O_4$ nanoparticles dispersed in the precursor solution. Under the



Please do not adjust margins

Please do not adjust margins



same conditions, $Fe_3O_4$ nanoparticles (8 nm diameter) were encapsulated into the **COF-TAPB-BTCA** superstructures, as confirmed by HAADF-STEM and HR-TEM images and XRPD (Figure 4a and S15 and S16, ESI†). The content of Fe in the composite was estimated by Inductively Coupled Plasma-Mass spectrometry (ICP-MS), from which a $Fe_3O_4$ content of 2.8 % w/w in the composite was determined. EDX mapping performed on a single superstructure showed the distribution of N, Fe and O atoms, confirming the presence of $Fe_3O_4$ into the superstructures (Figure 4c). Also, as indication of the encapsulation, a colloidal suspension of the composite was exposed to a magnet and rapidly attracted to it (Figure 4b). Similarly, magnetic measurements performed on the composite confirmed its magnetic character, exhibiting a characteristic hysteresis loop with a coercive field of 240 Oe at 10 K (Figure S17, ESI†).

In summary, we have reported a highly versatile and effective methodology to simultaneously synthesize and shaping microspherical hollow imine-based COF superstructures. This method also enables making COF-based composites by simple adding the selected functional materials during the spray-drying synthesis.

This work was supported by the EU FP7 ERC-Co 615954 and European Union's Horizon 2020 research and innovation program under grant agreement No. 685727. ICN2 acknowledges the support of the Spanish MINECO through the Severo Ochoa Centers of Excellence Program and the project MAT2016-77608-C3-1-P, under Grant SEV-2013-0295.

## Notes and references

1. P. J. Waller, F. Gándara and O. M. Yaghi, *Acc. Chem. Res.*, 2015, **48**, 3053-3063.
2. S.-Y. Ding and W. Wang, *Chem. Soc. Rev.*, 2013, **42**, 548-568.
3. J. Thote, H. Barike Aiyappa, R. Rahul Kumar, S. Kandambeth, B. P. Biswal, D. Balaji Shinde, N. Chaki Roy and R. Banerjee, *IUCrJ*, 2016, **3**, 402-407.
4. H. Furukawa and O. M. Yaghi, *J. Am. Chem. Soc.*, 2009, **131**, 8875-8883.
5. C. J. Doonan, D. J. Tranchemontagne, T. G. Glover, J. R. Hunt and O. M. Yaghi, *Nat Chem*, 2010, **2**, 235-238.
6. M. G. Rabbani, A. K. Sekizkardes, Z. Kahveci, T. E. Reich, R. Ding and H. M. El-Kaderi, *Chem. Eur. J.*, 2013, **19**, 3324-3328.
7. S. S. Han, H. Furukawa, O. M. Yaghi and W. A. Goddard, *J. Am. Chem. Soc.*, 2008, **130**, 11580-11581.
8. S.-Y. Ding, J. Gao, Q. Wang, Y. Zhang, W.-G. Song, C.-Y. Su and W. Wang, *J. Am. Chem. Soc.*, 2011, **133**, 19816-19822.
9. H. Li, Q. Y. Pan, Y. C. Ma, X. Y. Guan, M. Xue, Q. R. Fang, Y. S. Yan, V. Valtchev and S. L. Qiu, *J. Am. Chem. Soc.*, 2016, **138**, 14783-14788.
10. Q. R. Fang, S. Gu, J. Zheng, Z. B. Zhuang, S. L. Qiu and Y. S. Yan, *Angew. Chem. Int. Ed.*, 2014, **53**, 2878-2882.
11. G. Das, B. P. Biswal, S. Kandambeth, V. Venkatesh, G. Kaur, M. Addicoat, T. Heine, S. Verma and R. Banerjee, *Chem. Sci.*, 2015, **6**, 3931-3939.
12. Y. Yuan, H. Ren, F. X. Sun, X. F. Jing, K. Cai, X. J. Zhao, Y. Wang, Y. Wei and G. S. Zhu, *J. Mater. Chem.*, 2012, **22**, 24558-24562.
13. S.-Y. Ding, M. Dong, Y.-W. Wang, Y.-T. Chen, H.-Z. Wang, C.-Y. Su and W. Wang, *J. Am. Chem. Soc.*, 2016, **138**, 3031-3037.
14. S. Wan, J. Guo, J. Kim, H. Ihee and D. Jiang, *Angew. Chem.*, 2008, **120**, 8958-8962.
15. J. Mahmood, E. K. Lee, M. Jung, D. Shin, I.-Y. Jeon, S.-M. Jung, H.-J. Choi, J.-M. Seo, S.-Y. Bae, S.-D. Sohn, N. Park, J. H. Oh, H.-J. Shin and J.-B. Baek, *Nat. Commun.*, 2015, **6**, 6486.
16. H. Wei, S. Chai, N. Hu, Z. Yang, L. Wei and L. Wang, *Chem. Commun.*, 2015, **51**, 12178-12181.
17. D. Rodriguez-San-Miguel, A. Abrishamkar, J. A. R. Navarro, R. Rodriguez-Trujillo, D. B. Amabilino, R. Mas-Balleste, F. Zamora and J. Puigmarti-Luis, *Chem. Commun.*, 2016, **52**, 9212-9215.
18. B. P. Biswal, S. Chandra, S. Kandambeth, B. Lukose, T. Heine and R. Banerjee, *J. Am. Chem. Soc.*, 2013, **135**, 5328-5331.
19. P. Kuhn, M. Antonietti and A. Thomas, *Angew. Chem. Int. Ed.*, 2008, **47**, 3450-3453.
20. S. Karak, S. Kandambeth, B. P. Biswal, H. S. Sasmal, S. Kumar, P. Pachfule and R. Banerjee, *J. Am. Chem. Soc.*, 2017, **139**, 1856-1862.
21. Y. Peng, W. K. Wong, Z. Hu, Y. Cheng, D. Yuan, S. A. Khan and D. Zhao, *Chem. Mater.*, 2016, **28**, 5095-5101.
22. S. Furukawa, J. Reboul, S. Diring, K. Sumida and S. Kitagawa, *Chem. Soc. Rev.*, 2014, **43**, 5700-5734.
23. A. Carné-Sánchez, I. Imaz, K. C. Stylianou and D. Maspoch, *Chem. Eur. J.*, 2014, **20**, 5192-5201.
24. D. Rodriguez-San-Miguel, J. J. Corral-Perez, E. Gil-Gonzalez, D. Cuellas, J. Arauzo, V. M. Monsalvo, V. Carcelen and F. Zamora, *CrystEngComm*, 2017, **19**, 4872-4876.
25. J. Tan, S. Namuangruk, W. Kong, N. Kungwan, J. Guo and C. Wang, *Angew. Chem. Int. Ed.*, 2016, **55**, 13979-13984.
26. X. Shi, Y. Yao, Y. Xu, K. Liu, G. Zhu, L. Chi and G. Lu, *ACS Appl. Mater. Interfaces*, 2017, **9**, 7481-7488.
27. A. Halder, S. Kandambeth, B. P. Biswal, G. Kaur, N. C. Roy, M. Addicoat, J. K. Salunke, S. Banerjee, K. Vanka, T. Heine, S. Verma and R. Banerjee, *Angew. Chem. Int. Ed.*, 2016, **55**, 7806-7810.
28. S. Kandambeth, V. Venkatesh, D. B. Shinde, S. Kumari, A. Halder, S. Verma and R. Banerjee, *Nat. Commun.*, 2015, **6**, 6786.
29. A. Carné-Sánchez, I. Imaz, M. Cano-Sarabia and D. Maspoch, *Nat Chem*, 2013, **5**, 203-211.
30. L. Garzon-Tovar, M. Cano-Sarabia, A. Carne-Sanchez, C. Carbonell, I. Imaz and D. Maspoch, *React. Chem. Eng.*, 2016, **1**, 533-539.
31. V. Guillerm, L. Garzon-Tovar, A. Yazdi, I. Imaz, J. Juanhuix and D. Maspoch, *Chem. Eur. J.*, 2017, **23**, 6829-6835.
32. L. Garzón-Tovar, J. Pérez-Carvajal, I. Imaz and D. Maspoch, *Adv. Funct. Mater.*, 2017, **27**, 1606424.
33. L. Garzón-Tovar, S. Rodríguez-Hermida, I. Imaz and D. Maspoch, *J. Am. Chem. Soc.*, 2017, **139**, 897-903.
34. B. J. Smith, A. C. Overholts, N. Hwang and W. R. Dichtel, *Chem. Commun.*, 2016, **52**, 3690-3693.
35. A. de la Pena Ruigomez, D. Rodriguez-San-Miguel, K. C. Stylianou, M. Cavallini, D. Gentili, F. Liscio, S. Milita, O. M. Roscioni, M. L. Ruiz-Gonzalez, C. Carbonell, D. Maspoch, R. Mas-Balleste, J. L. Segura and F. Zamora, *Chem. Eur. J.*, 2015, **21**, 10666-10670.
36. D. Mullangi, S. Nandi, S. Shalini, S. Sreedhala, C. P. Vinod and R. Vaidhyanathan, *Sci. Rep.*, 2015, **5**, 10876.
37. D. Mullangi, S. Shalini, S. Nandi, B. Choksi and R. Vaidhyanathan, *Journal of Materials Chemistry A*, 2017, **5**, 8376-8384.
38. P. Wang, Q. Wu, L. Han, S. Wang, S. Fang, Z. Zhang and S. Sun, *RSC Advances*, 2015, **5**, 27290-27294.

 This journal is © The Royal Society of Chemistry 20xx

Please do not adjust margins